A Study of a Narrow Resonance 148 eV Above the ^{65}Cu$(p, n)^{65}$Zn Reaction Threshold*

D. W. Kneff, R. G. Clarkson,† and H. W. Lefevre
University of Oregon, Eugene, Oregon 97403

(Received 7 September 1972)

A thick target time-of-flight technique has been used to measure near-threshold neutrons from the ^{65}Cu$(p, n)^{65}$Zn reaction. The neutron yield near threshold is dominated by a narrow 2^- or 3^- ^{66}Zn resonance 148 eV above the 2.17-MeV reaction threshold. The c.m. angular distribution of resonance neutrons is isotropic to within 10%. Neutrons from this resonance lie within a forward cone of half angle 32° and have laboratory energies of 1180.9 ± 4.6 and 107.6 ± 0.6 eV for 0 and 180° c.m. angles, respectively. These energies, when combined with the known masses and reaction Q value, indicate a velocity decrease of 0.7% for the recoiling compound system before neutron decay. The product of the peak cross section and resonance width is 600 ± 50 mb eV, and the width is between 2 and 10 eV. Detailed balance predicts a ^{65}Zn$(n, p)^{65}$Cu cross section on the order of 1000 b at 144-eV neutron energy.

I. INTRODUCTION

In a previous paper on (p, n) reactions we pointed out that the Doppler energy resolution limit caused by thermal motion of target atoms depends on the proton velocity when energy measurements are made in the entrance channel and on the laboratory neutron velocity when energy measurements are made in the exit channel.[1] This limit strongly favors near-threshold neutron energy measurements in reactions with high negative Q values (Appendix A). In such reactions, direct neutron energy measurements provide a new set of windows for studying compound nucleus levels at high excitation energies with electron volt resolution. When Ref. 1 was written, however, we had not yet found a reaction with a resonance near enough to threshold to test the prediction that such resolution is obtainable.

In the course of measurements on several intermediate-weight nuclei, a strong, narrow resonance was found at a proton energy 148 eV above the 2.17-MeV ^{65}Cu$(p, n)^{65}$Zn reaction threshold (11.04 MeV in ^{66}Zn).[2] This paper presents the results of a study of that resonance.

II. ^{65}Cu$(p, n)^{65}$Zn TIME-OF-FLIGHT SPECTRA

Figure 1 is a ^{65}Cu$(p, n)^{65}$Zn neutron time-of-flight (TOF) spectrum produced by bombarding a thick, natural copper target with a nanosecond pulsed beam from the University of Oregon Van de Graaff accelerator. It was accumulated in about $4\frac{1}{2}$ h with an average beam current of 2 μA. The proton energy was about 15 keV above the 2.17-MeV reaction threshold. The detector was a 2-mm-thick, 7.6-cm-diam NE908 ^{6}Li-loaded glass scintillator, coupled to an RCA C70133B photomultiplier tube. The detector was placed at 0°, 10.6 cm from the target. The use of a thick target largely offset the low efficiency of the scintillator in the energy region of interest (1.6% at 1 keV and varying as $1/v$), since data were accumulated simultaneously for all neutron energies. The γ-ray sensitivity of the scintillator was reduced by setting a window on the ^{6}Li$(n, \alpha)^3$H pulse-height peak produced by keV neutrons. The signal-to-background ratio in such experiments is discussed in Appendix B.

Figure 1 contains several neutron peaks which indicate ^{66}Zn compound nucleus resonances and a γ-ray peak which was used to establish the time origin of the spectrum. The two prominent low-energy neutron peaks whose edges are labeled "forward" and "backward" are associated with a single ^{66}Zn compound nucleus level just above the reaction threshold; this resonance is the subject of this paper. The c.m. speed of the neutrons from the decay of the resonance is less than that of the c.m. In such a case all neutrons are emitted within a forward cone in the laboratory system. The two peaks are produced by forward and backward neutron emission in the c.m. system.

Figure 2 shows the geometrical relationship between the spatial distribution of resonance neutrons at a particular time t and the neutron detector. For a narrow resonance the neutrons can be described collectively in the laboratory system as a spherical shell that expands as it moves toward the detector. From Fig. 2 one may derive the relationship between the forward cone half angle, α, and the measured forward and backward laboratory neutron energies E_f and E_b, respectively:

$$\alpha = \sin^{-1}\left(\frac{\sqrt{E_f} - \sqrt{E_b}}{\sqrt{E_f} + \sqrt{E_b}}\right).$$

Similarly, the c.m. neutron energy is:

$$E_3' = \tfrac{1}{4}(\sqrt{E_f} - \sqrt{E_b})^2 .$$

A weighted average of six TOF measurements taken at different flight paths gave $E_f = 1180.9 \pm 4.6$ eV. A weighted average of four such measurements gave $E_b = 107.6 \pm 0.6$ eV. Thus $\alpha = 32.4 \pm 0.1°$ and $E_3' = 143.9 \pm 0.9$ eV for this resonance.

From Fig. 2 one can also see that neutrons produced in the reaction by protons nearer threshold than this resonance will appear between the forward and backward peaks in Fig. 1. The absence of neutrons between these two peaks shows that this resonance is the first ^{65}Cu$(p, n)^{65}$Zn resonance above the reaction threshold, and that the neutron yield between threshold and the resonance is inappreciable. From kinematics, the laboratory proton energy above threshold required to populate the resonance is related to the c.m. neutron energy by

$$\Delta E_p \equiv E_p - E_{\text{th}} = \frac{m_1 + m_2}{m_2} \frac{m_3 + m_4}{m_4} E_3' , \qquad (1)$$

where m_1, m_2, m_3, and m_4 are the proton, target nucleus, neutron, and residual nucleus rest masses, respectively. Hence $\Delta E_p = 148.4 \pm 0.9$ eV.

Since 148 eV is much smaller than the proton energy resolution in threshold measurements,[3-5] there is no observable resonance error[1] in such measurements. The discrepancy that has been noted from time to time between the Q value from threshold measurements and other measurement techniques[6,7] is not due to a resonance error in the threshold energy.

Referring again to Fig. 2, one can see that at short flight paths, where the flat detector subtends an angle larger than α, the detector will intercept all of the resonance neutrons. The geometrical relationship between the c.m. angle θ and the flight time t provides a simple means of measuring the c.m. angular distribution of resonance neutrons. The relationship is derived below and then compared with data taken at a short flight path.

From conservation of events,

$$N(t)dt = N(\Omega)d\Omega = N(\Omega)\frac{d\Omega}{dt}\,dt , \qquad (2)$$

where $N(t)dt$ is the number of neutrons incident upon the detector in a time interval dt at time t, and $d\Omega$ is the corresponding element of solid angle. For monoenergetic (c.m.) neutrons and a detector positioned axially at 0°

$$\cos\theta = \frac{L - V_{\text{c.m.}}t}{v't} . \qquad (3)$$

The variables are defined in Fig. 2. The transformation derivative is then

$$\frac{d\Omega}{dt} = -\frac{2\pi d(\cos\theta)}{dt} = \frac{2\pi L}{v't^2} .$$

The neutron flight time distribution thus varies as $1/t^2$ if $N(\Omega)$ is independent of angle. The observed distribution, which includes the variation of detector efficiency, $\epsilon(E_n)$, with neutron energy, is

$$N_{\text{observed}}(t)dt = N(\Omega)\frac{2\pi L\epsilon(E_n)}{v'}\frac{dt}{t^2} . \qquad (4)$$

The finite scintillator thickness and the velocity spread due to the natural resonance width are not included here. They broaden the otherwise sharp 0 and 180° c.m. edges.

Figure 3 shows a ^{65}Cu$(p, n)^{65}$Zn TOF spectrum

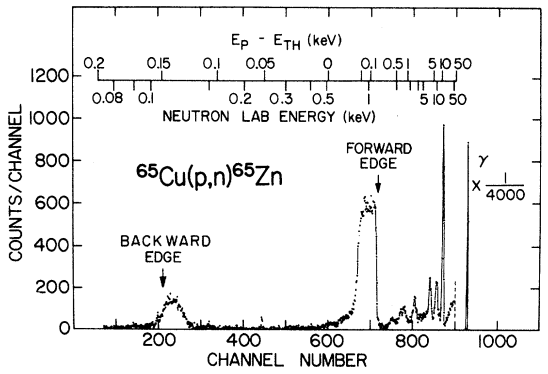

FIG. 1. Neutron TOF spectrum from a thick natural Cu target bombarded by protons of ~2185-keV energy. The flight path was 10.6 cm. A flat background of 36 counts per channel has been subtracted. The two prominent peaks whose edges are labeled "forward" and "backward" are from a single resonance 148 eV above threshold.

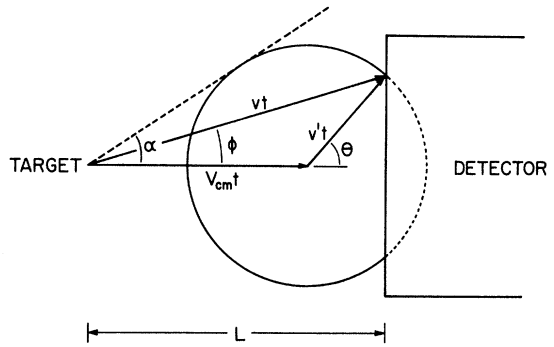

FIG. 2. Geometrical relationship between the spatial distribution of resonance neutrons at time t and the neutron detector. Neutrons from the resonance lie upon an expanding sphere whose center moves with the c.m. velocity. The neutron cone angle, α, is about 32° for the resonance discussed in the text.

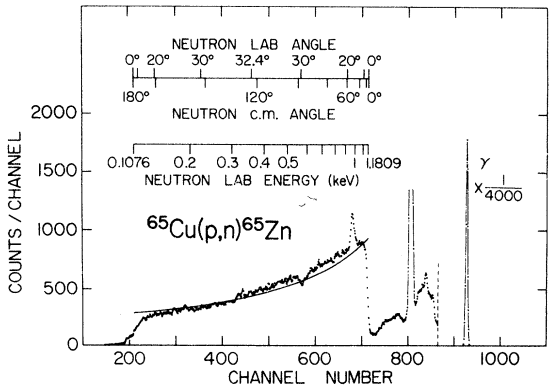

FIG. 3. Neutron TOF spectrum from a thick natural Cu target at a flight path of 5.3 cm. The detector intercepted all neutrons from the threshold resonance. A flat background of 90 counts per channel has been subtracted, and the data have been smoothed by a three-channel average. The solid curve is a TOF distribution generated for the resonance assuming that neutron emission is isotropic in the c.m. system. The peaks which appear in the data near channels 440 and 680 were produced by γ rays from incompletely suppressed proton bunches.

accumulated at a flight path of 5.3 cm. Here the detector intercepts all neutrons from the resonance. The solid curve in Fig. 3 was generated using Eq. (4) for an isotropic c.m. neutron yield [$N(\Omega)$ = constant]. It fits the data to within 10%. The tilt in the data relative to the generated distribution is attributed to neutron background from higher-energy resonances – to neutrons backscattered into the scintillator from the light pipe and photomultiplier tube. The dip in the data near channel 570 is due to a large neutron total cross-section resonance at 577 eV, associated with ^{63}Cu nuclei in the thick target. The peaks superimposed on the resonance yield near channels 440 and 680, and the large peak near channel 800, were produced by spurious γ rays created at the target by incomplete suppression of proton bunches in the accelerator beam pulsing system. Since the neutron flight path varies significantly with laboratory angle, the neutron energy scale in Fig. 3 has been corrected to account for this variation.

One concludes from the isotropic angular distribution that this ^{66}Zn compound nucleus resonance decays by s-wave neutron emission to the $(\frac{5}{2})^-$ ^{65}Zn ground state. The resonance is thus a 2^- or 3^- state, and can be populated by absorption of an s-wave or d-wave proton by the $(\frac{3}{2})^-$ ^{65}Cu ground state. A 2^- ^{66}Zn level can be populated by both s-wave and d-wave protons, and a 3^- level by the latter. The s-wave to d-wave proton penetrability ratio favors s-wave protons by a factor of 10 for this resonance. Note that if the state is a 2^- state, it is accessible via magnetic quadrupole excitation from the ^{66}Zn ground state using threshold photoneutron techniques.[8]

III. RESONANCE CROSS SECTION

$N(\Omega)$, the neutron yield per unit solid angle discussed in Sec. II, is clearly related to the reaction cross section. Its value, which we have determined by fitting the data in Fig. 3 (and our other data), is proportional to the integral over energy of the reaction cross section. The product of the c.m. resonance width, Γ, and the peak value, σ_p, of the total (p, n) reaction cross section (Appendix C) is

$$\Gamma\sigma_p = 8\,\frac{N(\Omega)}{N_p}\,\frac{1}{n}\,\frac{dE_p}{dx}\,,$$

where N_p is the number of protons incident upon the target. The value used for $(1/n)(dE_p/dx)$, the stopping cross section per ^{65}Cu atom in the target, was 2.79×10^{-14} eV cm^2, calculated from a 314-eV adjusted ionization potential.[9] The experimental value of $N(\Omega)$, increased by about 6% to correct for neutron scattering in the 1-mm-thick target, gives

$$\Gamma\sigma_p = 600 \pm 50 \text{ mb eV}.$$

The uncertainty is the mean square deviation of several experimental values.

The resonance width that we obtain (Sec. IV) is model dependent. It does have an upper bound of 8(±2) eV, however, which provides a lower limit to the peak cross section. The upper bound on the cross section was obtained from the maximum possible p + ^{65}Cu reaction cross section using equal proton and neutron partial widths for the compound state. The resultant bounds on the total reaction cross section at the peak of the resonance are

$$75\ (\pm20)\text{ mb} \leq \sigma_p \leq \begin{cases} 188 \text{ mb } (2^- \text{ compound state}) \\ 263 \text{ mb } (3^- \text{ compound state}) \end{cases}.$$

The large proton to neutron c.m. resonance energy ratio (1.48×10^4) points to a large cross section for the ^{65}Zn$(n, p)^{65}$Cu inverse reaction at this resonance. Using detailed balance and the above (p, n) results, the ^{65}Zn$(n, p)^{65}$Cu peak cross-section width product is

$$\sigma_{np}\,\Gamma = 5900 \pm 500 \text{ eV b}$$

and the peak cross section is bounded by

$$730\ (\pm200)\text{ b} \leq \sigma_{np} \leq \begin{cases} 1820 \text{ b } (2^- \text{ state}) \\ 2550 \text{ b } (3^- \text{ state}) \end{cases}.$$

This resonance occurs at 144 eV in the ^{65}Zn(n, p)-

^{65}Cu reaction. It seems likely that such surprisingly large (n, p) resonance cross sections could have a significant effect on some stellar synthesis rates.

IV. SLOWING DOWN AND THE RESONANCE WIDTH

Since the Q value for the ^{65}Cu$(p, n)^{65}$Zn reaction is known, it is clear that if free particle kinematics were obeyed, only three parameters would be required to described our data – the energy, width, and peak cross section of the resonance. Since, as we will show, the reaction does not obey free particle kinematics by a small but experimentally significant amount, at least four parameters are required to describe the data. The fourth parameter is a measure of the failure of free particle kinematics. This failure may be interpreted in several ways.

In order to obtain the forward and backward neutron energies quoted in Sec. II, we worked only in the exit channel. Line shapes were generated using forward *and* backward neutron energies and the resonance width as independent variables. The velocity of the c.m. was thus not constrained. Figure 4 shows a fit to the data of Fig. 1 with the c.m. resonance width, Γ, chosen to be 9 eV. The forward and backward neutron energies also obtained in this way were then compared with free particle kinematics.

Figure 5 is a plot of the variation of laboratory neutron energy with proton energy near the ^{65}Cu$(p, n)^{65}$Zn threshold. The shape of this kinematically generated curve is insensitive to the exact proton threshold energy. The rising portion of the curve describes 0° c.m. neutrons and the falling portion describes 180° c.m. neutrons. The laboratory neutron energy at threshold is 507 eV, and the neutron cone opens into 4π at a proton energy 523 eV above threshold. The dashed line in Fig. 5 denotes the position of the observed ^{65}Cu$(p, n)^{65}$Zn resonance as deduced from the measured neutron energies.

The inset of Fig. 5 expands the kinematics curve in the region of the resonance. It shows that the proton energies obtained from the two neutron energies disagree by 7.2 ± 2.4 eV. This disagreement has led us to collect additional data, and to search for systematic errors in the data and in its analysis. We can only conclude, as indicated above, that free particle kinematics fails for this reaction when studied at this resolution.

While one might attribute this energy discrepancy to an asymmetry in momentum transfer between the neutron and ^{65}Zn for forward and backward emission due to crystalline forces, we have confined our attention to a second alternative. From Fig. 2 it is apparent that if $V_{\text{c.m.}}$ decreases before neutron emission, both forward and backward laboratory neutron energies will also decrease. For this resonance, the observed neutron energies would yield the same proton energy above threshold[10] if the ^{66}Zn recoil nuclei had slowed down by 0.7% of their free particle velocity before decay. This would require a loss of about 470 eV of the compound system's original 33-keV free particle kinetic energy. As we will show later, this energy loss must occur over a ^{66}Zn

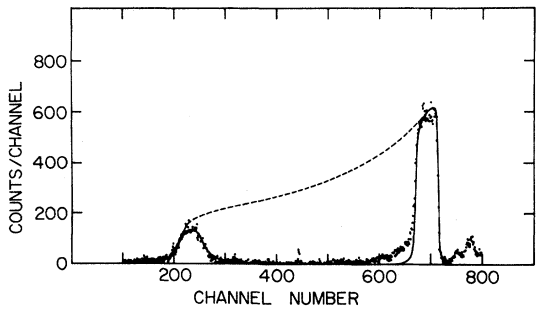

FIG. 4. Threshold resonance from the 10.6-cm spectrum overlapped with distribution curves generated for the entire resonance neutron yield (dashed curve) and for those neutrons intercepted by the detector (solid curve). These curves were generated with $\Gamma = 9$ eV.

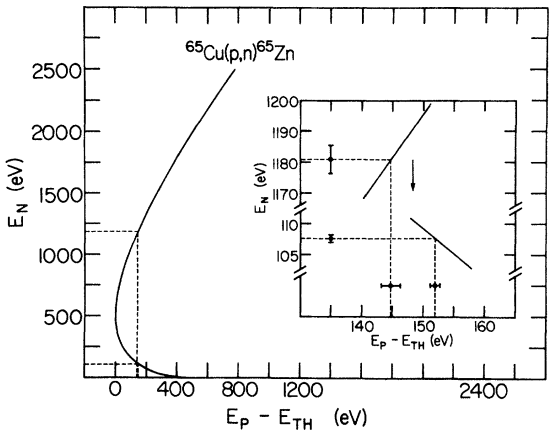

FIG. 5. Variation of laboratory neutron energy with proton energy at 0° near the ^{65}Cu$(p, n)^{65}$Zn reaction threshold. The rising portion of the curve describes forward c.m. neutrons and the falling portion describes backward c.m. neutrons. The dashed lines represent the position of the resonance of interest. The inset expands the curve in the vicinity of the resonance. The noncoincidence in proton energy indicates slowing down of the recoiling nucleus before neutron emission. The arrow in the inset denotes the proton energy above threshold calculated from Eq. (1), Sec. II of the text.

recoil distance that is only a fraction of the nearest neighbor distance (2.55 Å) in copper. Unfortunately, we cannot account for such a large loss of energy and momentum. Perhaps plasmon excitation could explain this loss.[11]

Any analysis used to obtain the width of the resonance must consider this failure of free particle kinematics. If the recoiling ^{66}Zn nuclei slow down after formation, classically they will have different velocities when they decay. This classical velocity spread introduces an additional energy spread in the laboratory neutron energies and thus broadens the observed resonance. The natural width, however, is directly related to the lifetime of the state through the uncertainty principle. For this particular resonance the velocity loss due to slowing down is comparable to the neutron velocity spread associated with the width of the state. In such a case one cannot expect classical behavior.

We can give limits on the width of the resonance without knowing the slowing down mechanism. Rather than presenting only the limits, however, we include a first-order analysis of the experimental resonance shape in terms of simple slowing down potentials. The analysis will show that the neutron spectrum is sensitive to details of the slowing down. This conclusion offers the possibility of an experimental study of the slowing down of slow heavy ions in a new time and distance regime (10^{-16} sec, 1 Å). It offers this possibility in a system where the initial position, velocity, and recoil direction with respect to a crystal lattice are well defined.

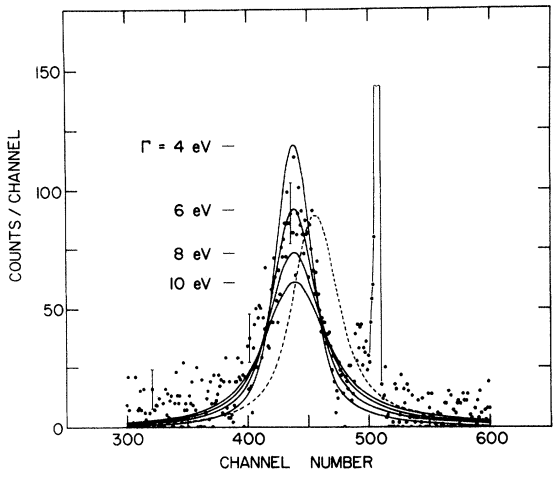

FIG. 6. Backward peak from a 19.1-cm TOF spectrum overlapped with several distribution curves. The solid curves were generated with free particle kinematics, but using effective target and compound nucleus masses 0.7% larger than the free particle masses. The dashed curve was generated using free particle masses and $\Gamma = 6.5$ eV. A flat background of 68 counts per channel has been subtracted from the data. The narrow peak near channel 510 was produced by γ rays from incompletely suppressed proton bunches.

A. Effective Mass

As noted above, the measured neutron energies indicate a recoil ^{66}Zn velocity 0.7% too small. One can reconcile this difference with kinematics by assigning an effective mass to the target nucleus (and thus to the compound nucleus) which is 0.7% larger than the free particle mass.[12] In terms of a slowing down potential this is equivalent to a δ function shaped potential well 470 eV deep. Neutron emission would occur after the recoiling nuclei had left the well. With this potential, slowing down does not contribute to the neutron energy spread. One thus obtains an upper limit to the natural width of the resonance. We interpret the value of Γ used to generate curves like that of Fig. 4 as such an upper limit.

Figure 6 shows a set of line shapes generated to overlap the backward peak of a spectrum obtained with a 19.1-cm flight path. The solid curves were generated with Breit-Wigner distributions of various c.m. widths. Time spreads due to the detector solid angle (0.12 sr) have been included. Each curve was normalized to the measured cross-section width product. $\Gamma = 6.5$ eV appears to fit these data best. Fits to 10.6-, 11.2-, and 19.1-cm spectra yielded a width of 8 ± 2 eV. Figure 6 also includes a dashed curve generated with free particle kinematics and with the free particle masses for $\Gamma = 6.5$ eV. The dashed curve shows where the peak would have to be if free particle kinematics were obeyed.

The 8 ± 2-eV upper limit on the resonance width corresponds to a compound nucleus lifetime of $(8 \pm 2) \times 10^{-17}$ sec. In this time a recoiling ^{66}Zn nucleus travels about 0.25 Å. A 2.3 ± 0.2-eV lower limit to the resonance width is obtained by combining the measured cross-section width product with the maximum possible cross section (Sec. III). The lower limit on Γ corresponds to a lifetime of $(2.9 \pm 0.3) \times 10^{-16}$ sec and a recoil distance of about 1 Å.

B. Continuous Slowing Down

Here we assume that the ^{66}Zn nuclei slow down continuously between formation and decay. We consider two slowing down potentials: a triangular potential, which gives uniform acceleration, and a parabolic potential, which gives an acceleration nearly proportional to the time, since the fractional change in velocity before neutron emission is small. We choose the system in which the

^{66}Zn nucleus is at rest immediately after formation as the reference frame. This is the free particle c.m. frame. In this frame the potential well moves past the nucleus with an initial velocity $-\vec{V}_{c.m.}$.

The time- and angle-dependent neutron resonance energy in this reference frame is

$$E_0' = \tfrac{1}{2} m_3 [\vec{v}' + \vec{V}'(t)]^2 ,$$

where $\vec{v}'$ is the unperturbed c.m. neutron velocity and $\vec{V}'(t)$ is the velocity of the compound nucleus relative to the reference frame. For uniform acceleration

$$\vec{V}'(t) = -\vec{\alpha} t ,$$

where $\vec{\alpha}$ is a constant, directed parallel to $\vec{V}_{c.m.}$. For harmonic slowing down,

$$\vec{V}'(t) = \vec{V}_{c.m.} \left\{ \cos\left[\left(\frac{k}{m_c} \right)^{1/2} t \right] - 1 \right\} ,$$

where k is an effective spring constant and m_c is the mass of the compound system. Note that here also $\vec{V}'(0) = 0$.

In order to calculate the neutron spectrum quantum mechanically, we regard the neutron emission as time coherent. For a state of natural width Γ, the time dependence of the probability amplitude for emission (in the absence of slowing down) is given by

$$A(t) = e^{-(i/\hbar)(E_0 + i\,\Gamma/2)t} .$$

For our problem of emission from an accelerated radiator we replaced the unperturbed c.m. neutron energy E_0 by E_0', as given above.[13] $A(t)$ was then Fourier-transformed numerically and multiplied by its complex conjugate to obtain points on the c.m. neutron energy and angular distribution:

$$|\phi(E, \cos\theta)|^2 = \left| \int_0^\infty e^{-(i/\hbar)(E - E_0')t} e^{-(\Gamma/2\hbar)t}\, dt \right|^2 .$$

The neutron arrival time distribution at the scintillator was calculated for 2.4-mm annular zones and summed to obtain the laboratory line shape.

Figure 7 shows the best-matching line shapes generated for the 19.1-cm data. The dashed curve was generated with uniform slowing down, for parameter values $\Gamma = 6.5 \pm 0.5$ eV and $\vec{\alpha} = (1.3 \pm 0.3) \times 10^{-3} \vec{V}_{c.m.} \Gamma/\hbar$. Γ and α were varied to obtain the best overlap with the data. The solid curve in Fig. 7 is for harmonic slowing down, with parameter values $\Gamma = 2.0 \pm 0.5$ eV and $k = 300 \pm 100$ eV/Å^2. In both cases the stated uncertainties represent the sensitivity of the curves to parameter variations: A change in any parameter by its quoted uncertainty gives a noticeably less satisfactory overlap with the data. Again each curve was normalized to the measured cross-section width product.

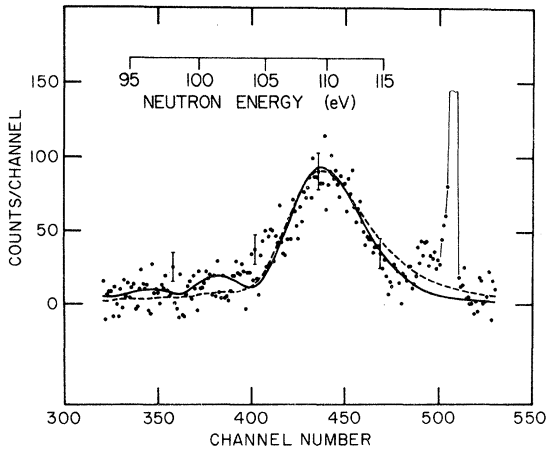

FIG. 7. Best overlap to the data of Fig. 6 obtained assuming continuous slowing down of the compound nucleus before neutron emission. The dashed curve is for uniform slowing down; $\Gamma = 6.5$ eV and the compound system slows down 0.13% in the first lifetime. The solid curve is for harmonic slowing down; $\Gamma = 2$ eV and the spring constant is 300 eV/Å^2. The flight time through the scintillator (14 channels) has not been folded in. The ordinate scale origin corresponds to a flat background of 68 counts per channel. The neutron energy scale assumes an axial flight path and is thus for reference purposes only.

A feature of both of these line shapes is the presence of oscillations on the low-energy tails. In the uniform case the oscillations were largely averaged out in the calculation by the detector geometry. Statistically, one cannot say whether or not oscillations are present in the data. Also, our use of a polycrystalline target may have averaged them out in the experiment.

We conclude, from the noticeably different shapes of the curves generated with the two continuous slowing down potentials, and with the effective mass assumption, that the TOF backward peak does provide information on the slowing down. The statistics of the present data do not allow us to reject any of the potentials we have tried. If interference oscillations are found, however, their amplitude and wavelength would greatly aid in characterizing the slowing down. It thus might be helpful to describe the position of interference maxima with reference to Fig. 2 at that particular time t. The maxima lie on spheres with the same radius as that in Fig. 2. The centers of those spheres are displaced progressively left from the center of the sphere shown there.

TABLE I. The first resonance above the $^{65}Cu(p,n)^{65}Zn$ reaction threshold.

Proton energy above threshold: 148.4 ± 0.9 eV
(Threshold proton energy: 2168.0 ± 0.8 keV [a])
c.m. neutron energy: 143.9 ± 0.9 eV
Laboratory 0° resonance neutron energies: 1180.9 ± 4.6 eV (0° c.m.) 107.6 ± 0.6 eV (180° c.m.)
Neutron laboratory cone half angle $\approx 32°$
Spin and parity: 2^- or 3^-
$\Gamma\sigma_p$: 600 ± 50 mb eV
Width: $8(\pm 2)$ eV $\geq \Gamma \geq 2.3(\pm 0.2)$ eV
Lifetime: $(8 \pm 2) \times 10^{-17}$ sec $\leq \tau \leq (2.9 \pm 0.3) \times 10^{-16}$ sec
^{66}Zn recoil distance in one lifetime: 1 Å $\gtrsim d \gtrsim 0.25$ Å
Reaction cross section at resonance peak: $75\ (\pm 20)$ mb $\leq \sigma_p \leq \begin{cases} 188 \text{ mb } (2^- \text{ state}) \\ 263 \text{ mb } (3^- \text{ state}) \end{cases}$
Inverse reaction cross section at resonance peak: $730\ (\pm 200)$ b $\leq \sigma_{np} \leq \begin{cases} 1820 \text{ b } (2^- \text{ state}) \\ 2550 \text{ b } (3^- \text{ state}) \end{cases}$

[a] Reference 5.

V. SUMMARY

Table I summarizes the characteristics of the first resonance above the $^{65}Cu(p,n)^{65}Zn$ reaction threshold.

Parks *et al.*[14] have suggested the use of a narrow, well isolated $^{37}Cl(p,n)$ or $^{40}Ar(p,n)$ resonance as a proton accelerator energy calibration point to replace the $^{7}Li(p,n)^{7}Be$ threshold standard, which is reliable only to within ±1 keV. The observed $^{65}Cu(p,n)^{65}Zn$ thick target threshold is dominated by the resonance 148 eV above the true threshold. This apparent threshold is an ideal candidate for a calibration point for proton energies in the vicinity of 2.17 MeV. Its application requires an absolute velocity gauge measurement.[15] Note that since the integral yield curve is a resonance integral curve, an $E^{3/2}$ extrapolation is not correct for determining a Q value. The rise of the integral yield in such measurements is completely dominated by energy spreads in the proton beam and by Doppler effects in the copper target.

VI. ACKNOWLEDGMENTS

The authors wish to thank J. C. Overley for his continuing interest in this work and for helpful suggestions during many discussions. C. A. Burke and M. T. Lunnon contributed during data collection. W. Schulz and J. D. MacDonald provided valuable technical assistance. G. Mahan has been a helpful consultant.

APPENDIX A: DOPPLER LIMIT

The entrance channel proton velocity is the sum of the laboratory proton velocity and the velocity of the thermally agitated target nucleus with which it interacts. The entrance channel proton energy spread introduced by the random direction of motion of the target nuclei is proportional to the cross term in the square of the velocity sum. For an ideal gas this is $\pm 2(E_1 m_1 kT/m_2)^{1/2}$, where $kT = E_2$, subscripts 1 and 2 refer to the incident and target nuclei, respectively, k is the Boltzmann constant, and T is the temperature. This result matches the Gaussian standard deviation in Bethe's more detailed derivation.[16] Making this identification and incorporating Lamb's replacement of kT by $\bar{\epsilon}$, the average energy per vibrational degree of freedom of a crystalline target (in the case of weak lattice binding),[17] the entrance channel Gaussian Doppler resolution limit full width at half maximum (FWHM) becomes

$$4(\ln 2)^{1/2} \left(\frac{E_1 m_1 \bar{\epsilon}}{m_2} \right)^{1/2}.$$

The measured exit channel neutron velocity is the sum of the velocity of the neutron emitted from the recoiling compound nucleus and the random thermal velocity the compound nucleus has

carried along from the instant of its formation. The corresponding exit channel Gaussian Doppler energy resolution limit FWHM becomes

$$4(\ln 2)^{1/2}\left(\frac{E_3 m_3 E_c}{m_c}\right)^{1/2} \approx 4(\ln 2)^{1/2}\left(\frac{E_3 m_3 \bar{\epsilon}}{m_2}\right)^{1/2},$$

where $E_c \approx E_2 = \bar{\epsilon}$ and $m_c \approx m_2$. Subscripts c and 3 refer to the compound nucleus and the neutron, respectively.

The entrance channel-to-exit channel ratio of the above Doppler energy resolution limits is approximately $(E_1/E_3)^{1/2}$. This is nearly the laboratory velocity ratio.

APPENDIX B: RESONANCE SIGNAL-TO-BACKGROUND RATIO

For a threshold resonance, the ratio of the height of the resonance peak to the background (signal-to-background ratio) in a neutron TOF spectrum varies with either $1/L$, $1/L^2$, or $1/L^3$, where L is the flight path. We assume that the width of each time channel is constant, and that the background rate is independent of detector position. At a short flight path the peak width depends on the detector solid angle while the peak height does not. For small flight path variations, the signal-to-background ratio thus depends only on the rate of arrival of the resonance neutrons at the detector, and is thus proportional to $1/L$. At longer flight paths, in those cases where the observed width of the peak is dominated by the flight time through the scintillator or the instrumental timing resolution, the peak width is independent of flight path. The signal-to-background ratio then varies as the detector solid angle, or as $1/L^2$. Increasing the flight path still more improves energy resolution while the scintillator thickness and instrumental timing resolution factors remain constant. Thus the natural resonance width can become dominant at long flight paths. In that case the signal-to-background ratio depends on both the rate of arrival of the neutrons and on the detector solid angle, and is proportional to $1/L^3$.

We also wish to point out that moderation of the neutrons near the scintillator should be avoided. The plastic light pipe used to couple the flat scintillator to the curved face plate of our photomultiplier tube was replaced by a specially fabricated glass light pipe[18] for part of the measurements reported here. The improvement in signal-to-background ratio was about a factor of 3.

APPENDIX C: RESONANCE CROSS SECTION

When N_p protons are incident upon a thin target, the number of neutrons, N, emitted into an element of solid angle $d\Omega$ is given by

$$N = N_n(E_p, \theta)dE_p d\Omega = N_p \sigma_{E_p}(\theta) d\Omega\, n\, dx\,. \tag{C1}$$

Here E_p is the proton energy, θ is the laboratory angle between the beam direction and the emitted neutrons, $n\,dx$ is the areal density of productive target atoms, and $\sigma_{E_p}(\theta)$ is the differential cross section at angle θ. After rearranging, we have

$$\sigma_{E_p}(\theta)dE_p d\Omega = \frac{N_n(E_p, \theta)dE_p d\Omega}{N_p}\left(\frac{1}{n}\frac{dE_p}{dx}\right). \tag{C2}$$

Note that $(1/n)(dE_p/dx)$ is the stopping cross section per ^{65}Cu atom in the target, where dE_p is the energy loss associated with atoms of all types in the layer of thickness dx.

If the incident proton energy is greater than that necessary to excite an isolated (p, n) resonance, and the target is sufficiently thick, the protons will slow down through the entire resonance. The total (p, n) cross section is obtained by integrating Eq. (C2) over the resonance for all energies and angles. For an isotropic c.m. neutron yield, integration over angles for the left and right sides, respectively, of Eq. (C2) gives

$$\int_0^{2\pi}\int_0^{\pi} \sigma_{E_p}(\theta)dE_p \sin\theta\, d\theta d\phi = 4\pi\sigma_{E_p}(\theta_{\text{c.m.}})dE_p = \sigma_{E_p}dE_p \tag{C3}$$

and

$$\frac{1}{N_p}\left(\frac{1}{n}\frac{dE_p}{dx}\right)\int_0^{2\pi}\int_0^{\pi} N_n(E_p, \theta)dE_p \sin\theta\, d\theta d\phi = \frac{1}{N_p}\left(\frac{1}{n}\frac{dE_p}{dx}\right)4\pi N(E_p, \Omega)dE_p, \tag{C4}$$

where $\sigma_{E_p}(\theta_{\text{c.m.}})$ is the differential cross section for c.m. angle $\theta_{\text{c.m.}}$, σ_{E_p} is the total resonance cross section at E_p, and $N(E_p, \Omega)dE_p$ is the neutron yield per unit c.m. solid angle. We have made use of the fact that the integrals over all angles of the differential cross section and of the differential neutron yield are the same for both the laboratory and c.m. systems. Assuming a Breit-Wigner resonance shape with a

peak cross section σ_p and a FWHM Γ, direct integration of Eq. (C3) over energy shows that

$$\int_{-\infty}^{\infty} \sigma_{E_p} dE_p = \tfrac{1}{2}\pi\Gamma\sigma_p \,. \tag{C5}$$

For a narrow resonance width, the integral of Eq. (C4) becomes

$$\int_{-\infty}^{\infty} \frac{1}{N_p}\left(\frac{1}{n}\frac{dE_p}{dx}\right) 4\pi N(E_p,\Omega)dE_p \approx \frac{1}{N_p}\left(\frac{1}{n}\frac{dE_p}{dx}\right) 4\pi \int_{-\infty}^{\infty} N(E_p,\Omega)dE_p = 4\pi\,\frac{N(\Omega)}{N_p}\left(\frac{1}{n}\frac{dE_p}{dx}\right) . \tag{C6}$$

$N(\Omega)$ is the total neutron yield per unit solid angle. Combining Eqs. (C5) and (C6) gives the total cross section at the peak of the resonance:

$$\sigma_p = \frac{8}{\Gamma}\,\frac{N(\Omega)}{N_p}\left(\frac{1}{n}\frac{dE_p}{dx}\right) . \tag{C7}$$

This is the result used in the text.

---

*Work supported in part by the U. S. Atomic Energy Commission and the National Science Foundation.

†Present address: Nuclear Physics Research Unit, University of the Witwatersrand, Johannesburg, South Africa.

[1]D. W. Kneff, H. W. Lefevre, and G. U. Din, Phys. Rev. Letters 25, 1210 (1970).

[2]H. W. Lefevre, D. W. Kneff, and R. G. Clarkson, Bull. Am. Phys. Soc. 16, 626 (1971).

[3]K. Okano and K. Nishimura, J. Phys. Soc. Japan 18, 1563 (1963).

[4]C. H. Johnson, C. C. Trail, and A. Galonsky, Phys. Rev. 136, B1719 (1964).

[5]J. C. Overley, P. D. Parker, and D. A. Bromley, Nucl. Instr. Methods 68, 61 (1969).

[6]S. C. Pancholi and K. Way, Nucl. Data B2(No. 6), 29 (1968); see also Ref. 3.

[7]J. B. Marion and R. A. Chapman, Phys. Rev. 101, 283 (1956).

[8]C. D. Bowman, G. S. Sidhu, and B. L. Berman, Phys. Rev. 163, 951 (1967); B. L. Berman, G. S. Sidhu, and C. D. Bowman, Phys. Rev. Letters 17, 761 (1966).

[9]J. E. Turner, in *Studies in Penetration of Charged Particles in Matter*, Nuclear Science Series Report No. 39 (National Academy of Science-National Research Council, Washington, D. C., 1964), p. 99.

[10]That energy given by Eq. (1). Note that Eq. (1) is exact even in the presence of slowing down.

[11]See, for example, C. Kittel, *Introduction to Solid State Physics* (Wiley, New York, 1966), 3rd ed., p. 233.

[12]If one instead tries to reconcile the difference by adjusting the reaction Q value, the resulting Q value is 31 keV less negative than that deduced from threshold measurements (Ref. 5). The required adjustment is 6 times larger than the spread between experimentally derived Q values (Refs. 3–7).

[13]If one were working from first principles the time dependence of E_0' would have to be included in the time-dependent Schrödinger equation before solving that equation for $A(t)$. See, for example, E. Merzbacher, *Quantum Mechanics* (Wiley, New York, 1961).

[14]P. B. Parks, P. M. Beard, E. G. Bilpuch, and H. W. Newson, Nucl. Phys. 85, 504 (1966).

[15]J. D. Seagrave, J. E. Brolley, Jr., and J. G. Beery, Rev. Sci. Instr. 35, 1290 (1964); M. L. Roush, L. A. West, and J. B. Marion, Nucl. Phys. A147, 235 (1970).

[16]H. A. Bethe and G. Placzek, Phys. Rev. 51, 450 (1937); H. A. Bethe, Rev. Mod. Phys. 9, 69 (1937).

[17]W. E. Lamb, Jr., Phys. Rev. 55, 190 (1939).

[18]John Unertl Optical Company, Pittsburgh, Pa. 15214.